Available online at www.sciencedirect.com
SCIENCE DIRECT
Journal of Catalysis 231 (2005) 67–76
JOURNAL OF CATALYSIS
www.elsevier.com/locate/jcat

Sn-modified Ni catalysts for aqueous-phase reforming: Characterization and deactivation studies

J.W. Shabaker, D.A. Simonetti, R.D. Cortright, J.A. Dumesic *

Department of Chemical and Biological Engineering, University of Wisconsin, Madison, WI 53706, USA

Received 19 August 2004; revised 6 January 2005; accepted 16 January 2005

Abstract

The catalytic deactivation of R-NiSn catalysts was explored during hydrogen production by aqueous-phase reforming (APR) of ethylene glycol. X-ray photoelectron spectroscopy and CO and H_2 adsorption microcalorimetry were combined with previous characterization to show that R-NiSn catalysts are composed of a Ni core surrounded by a Ni_3Sn alloy after heat treatments above 533 K. Adsorption studies (CO, H_2, and N_2), XPS, X-ray diffraction, and thermogravimetric analysis show that R-$Ni_{15}Sn$ catalysts deactivate by interaction with water under APR reaction conditions, rather than coking or $Ni(CO)_4$ formation. Over the first 48 h on stream, deactivation proceeds rapidly by the sintering of small Ni particles and by the formation of NiSn surface alloys with lower catalytic activity and higher selectivity for the production of hydrogen by APR of dilute feed solutions. After several days on stream, R-$Ni_{15}Sn$ catalysts deactivate at a slower rate because of oxidation and dissolution by water, leading to Ni effluent concentrations near 50 wppm after 240 h on stream. The first-order deactivation constant can be improved from $k_d = 0.0020$ h^{-1} to less than 0.0001 h^{-1} between 140 and 240 h on stream with the use of rigorous heat treatments at 623 K in H_2 to form resilient NiSn alloys prior to reaction and/or with the use of energy-efficient stoichiometric feeds (water/ethylene glycol = 2).

Keywords: Ethylene glycol; Reforming; Hydrogen production; Nickel–tin catalysts; Microcalorimetry; XPS; Catalyst deactivation

1. Introduction

The production of hydrogen is a major limitation in the widespread use of fuel cells for the generation of electricity. Aqueous-phase reforming (APR) produces hydrogen in a single liquid-phase reactor at temperatures near 500 K. This process can use low-cost, renewable oxygenated hydrocarbons derived from biomass (e.g., sorbitol, glycerol, ethylene glycol) that are environmentally benign [1–3]. The APR reaction proceeds through a carbon monoxide intermediate:

$$\text{Reforming: } C_2H_6O_{2(l)} \rightleftarrows 2CO_{(g)} + 3H_{2(g)}, \quad (1)$$

$$\text{WGS: } CO_{(g)} + H_2O_{(l)} \rightleftarrows CO_{2(g)} + H_{2(g)}, \quad (2)$$

$$\text{APR: } C_2H_6O_{2(l)} + 2H_2O_{(l)} \rightleftarrows 2CO_{2(g)} + 5H_{2(g)}. \quad (3)$$

Early work proved that high activity, selectivity, and stability for hydrogen production could be achieved with Pt-based catalysts [4–6]. Further studies have detailed the development of inexpensive Sn-promoted Raney Ni catalysts with similar activity and selectivity for aqueous-phase reforming of oxygenated hydrocarbons as Pt/Al_2O_3 [7–9]. Although these Raney Ni-based catalysts deactivate much more slowly than supported Ni catalysts, which have been shown to sinter rapidly under APR process conditions [8], they partially deactivate over a period of days during the aqueous-phase reforming of dilute solutions of oxygenated hydrocarbons at temperatures near 500 K. In addition to sintering in the aqueous environment, Ni-based catalysts are vulnerable to oxidation (by dissolved oxygen or water) and metal loss by leaching into the reactor effluent. Finally, Ni-based catalysts are vulnerable to strong interactions with feed molecules and reaction intermediates of the APR process that may lead to catalyst deactivation by coking.

* Corresponding author.
E-mail address: dumesic@engr.wisc.edu (J.A. Dumesic).

0021-9517/$ – see front matter
doi:10.1016/j.jcat.2005.01.019

In this paper we report the results of characterization of R-NiSn catalysts by X-ray photoelectron spectroscopy (XPS), adsorption studies, and thermogravimetric analysis (TGA) to assess the state of the fresh and spent catalysts. We then present the results of long-term catalytic stability tests to quantify the deactivation of R-NiSn catalysts and suggest process conditions that stabilize their performance considerably during aqueous-phase reforming.

2. Experimental

2.1. Catalyst preparation

We prepared Raney Ni–Sn (R-Ni$_x$Sn) catalysts by reducing Raney Ni 2800 (R-Ni) (Grace Davison) at 533 K for 2 h (heating at 0.5 K min^{-1}) in flowing H_2, adding appropriate amounts of a 9.4 wt% Sn (tributyltin acetate) solution in ethanol to reduced R-Ni under a N_2 atmosphere, and subsequently heating the mixture in a sealed Parr acid digestion bomb to 423 K for 2 h (heating at 0.5 K min^{-1}). The catalysts were then washed and stored under de-ionized water. Before characterization or collection of reaction kinetics data, all catalysts were reduced in flowing H_2 (100 cm^3(STP) min^{-1}) for 2 h at 533 K, unless noted otherwise. We passivated some catalysts for characterization by flowing 2% O_2/He mixtures at 300 K. The composition of each fresh catalyst was verified by atomic absorption spectroscopy (AAS/ICP) after digestion in acids.

2.2. Reaction kinetics measurements

Reaction kinetics measurements were performed to quantify catalyst deactivation with a reactor system described elsewhere [5]. The Raney catalysts were loaded without sieving (particle diameters are 45–90 μm) or pelletizing to operate in the kinetic regime [5]. De-aerated aqueous solutions containing 5–63 wt% ethylene glycol were fed to the reactor at a flow rate of 0.08 cm^3 min^{-1}. Reaction kinetics measurements were made at temperature of 483 K and system pressures near the bubble-point of the feed solution. Each reaction condition was maintained for at least 6 h to ensure that steady state had been achieved, as determined by online gas chromatography. The liquid-phase effluent from the reactor was collected during reaction kinetics measurements, and this liquid was analyzed via gas chromatography (FID detector), total organic carbon (TOC), and atomic absorption (AAS/ICP) measurements. The "normalized CO_2 activity" (current CO_2 production rate/initial CO_2 production rate) was used to assess catalyst stability.

2.3. Catalyst characterization

Freshly reduced catalysts were characterized by N_2 adsorption at 77 K (BET method) and the irreversible extent of CO adsorption at 300 K. Spent catalysts were similarly characterized by adsorption studies after drying in air at 300 K (after runs with 5 wt% ethylene glycol feed solutions) or at 373 K (after runs with 63 wt% ethylene glycol feed solutions) and subsequent reduction at 523 K for 2 h (0.5 K min^{-1}). X-ray diffraction studies were conducted with a Cu-K_α source and a Scintag PADV diffractometer operating at 40.0 mA and 35.0 kV. The Scherrer equation was used to estimate the Ni crystal size. Fresh catalysts were reduced and passivated in flowing 2% O_2/He before XRD, and spent catalysts were dried under air as described above.

The procedure for microcalorimetry has been described in detail elsewhere [10]. Briefly, passivated R-NiSn catalysts were reduced for 2 h at 523 K in a quartz flow cell under H_2 (200 cm^3(STP) min^{-1}, ultrahigh purity) after heating at 1.3 K min^{-1}. The cell was then sealed and evacuated for 5 min before introduction of flowing He (200 cm^3(STP) min^{-1}, ultrahigh purity). The cell was then purged with He for 1 h at 523 K before the sample was torch-sealed inside a Pyrex NMR tube for transport to the microcalorimeter. Microcalorimetry of CO and H_2 adsorption was performed at 300 K on separate samples of each catalyst with a Setaram BT2.15D heat-flux calorimeter.

Before we collected XPS spectra, samples were treated in a high-vacuum pretreatment cell. Samples were dropped onto Ta sample plates in slurry form. Each sample plate was manually loaded onto a heater stage in a pretreatment cell and dried there under flowing H_2 or N_2 for 2 h at 333 K. Once dry, most samples were treated at elevated temperature in flowing H_2 (100 cm^3(STP) min^{-1}, ultrahigh purity). The pretreatment cell was then evacuated to < 0.3 Torr with a dry diaphragm pump, and the reduced or oxidized sample was transferred into a UHV system with a base pressure below 10^{-10} Torr via a turbopump-evacuated load-lock without exposure to air. The XPS system irradiated the sample with a 400-W Mg (K_α) X-ray gun, and photoelectrons were collected with an Omicron EA 125 Channeltron energy analyzer. The spectrometer was calibrated to the Ag $4s^{1/2}$ line at a binding energy of 97.0 eV. Surface compositions were measured with the use of the Ni $2p^3$, Sn $3d^5$, C 1s, O 1s, and Al 2p peak areas and sensitivities published elsewhere [11].

Thermogravimetric analysis was accomplished with a Netzsch TG 209 apparatus. Approximately 20 mg of each catalyst was loaded into an Al sample boat and placed on the balance. The sample zone was then sealed and purged with N_2 (40 cm^3(STP) min^{-1}) for 30 min before it was heated to 493 K (10 K min^{-1}) and held for 1 h. The dried sample was then heated to 823 K (10 K min^{-1}) and held for 10 min. After cooling to 278 K under flowing N_2, the flowing gas was switched to air (40 cm^3(STP) min^{-1}) and allowed to purge for 30 min. The sample was then heated directly to 823 K (10 K min^{-1}) in air and held for 10 min.

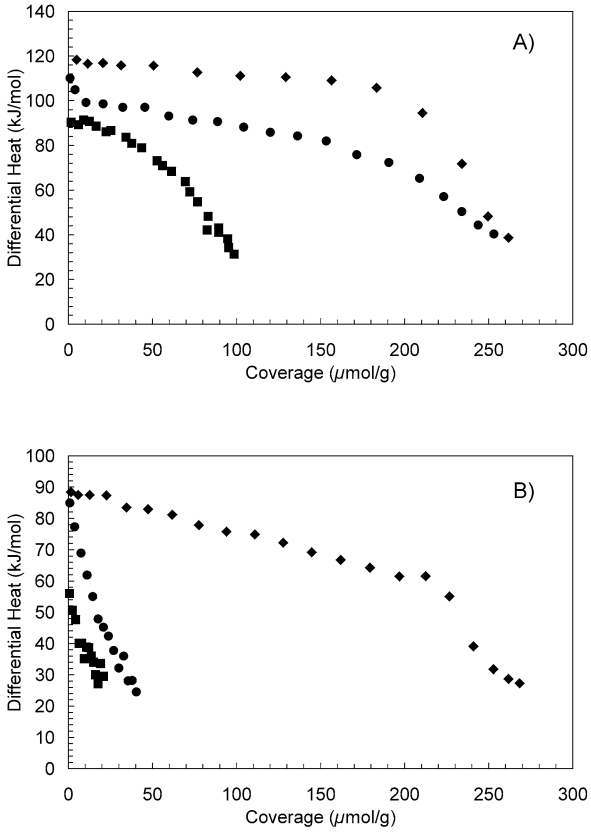

Fig. 1. Differential heat of (A) carbon monoxide and (B) H_2 adsorption at 300 K on R-Ni (♦), R-$Ni_{14}Sn$ (●), and R-Ni_4Sn (■).

3. Results

3.1. Microcalorimetric studies

Microcalorimetry results for the adsorption of carbon monoxide and hydrogen at 300 K on R-Ni-based catalysts are shown in Fig. 1. The initial heat of adsorption of CO decreases from about 120 kJ mol^{-1} for R-Ni to near 110 and 90 kJ mol^{-1} for R-$Ni_{14}Sn$ and R-Ni_4Sn, respectively. The initial heat of H_2 adsorption also decreases with Sn addition, with values of 90, 85, and 55 kJ mol^{-1} for R-Ni, R-$Ni_{14}Sn$, and R-Ni_4Sn, respectively. The R-$Ni_{14}Sn$ catalyst shows a small fraction of strong adsorption sites (less than 20 μmol CO g^{-1}) that resemble pure R-Ni.

3.2. X-ray photoelectron spectroscopy

In situ XPS results for Raney-Ni-based catalysts after various treatments are given in Figs. 2 and 3; the corresponding surface compositions are listed in Table 1. Core-level Ni spectra (Fig. 2) show that R-Ni is fully reduced to Ni^0 after treatment in H_2 for 2 h at 533 K. The Ni $2p^{3/2}$ line appears at a binding energy of 852.8 eV. In contrast, freshly prepared R-$Ni_{14}Sn$ that is dried under air contains a NiO_x species with a binding energy of 856.4 eV. This species may be a hydrated Ni species, since pure NiO is usually found

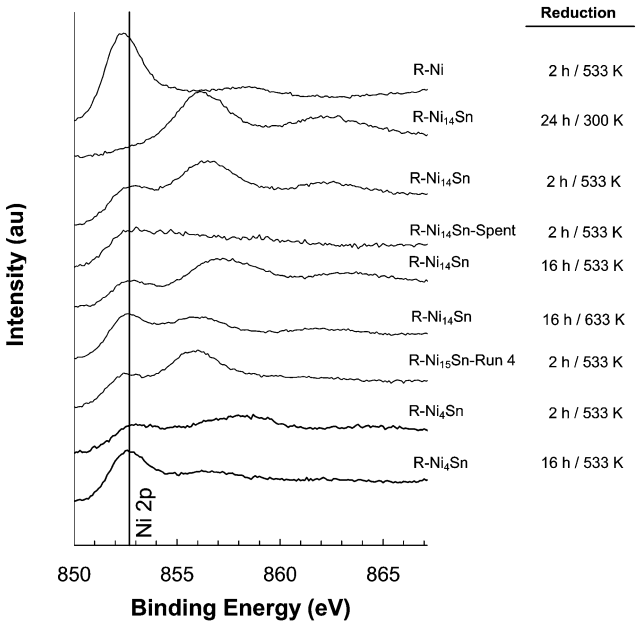

Fig. 2. Ni 2p region of X-ray photoelectron spectra of R-NiSn catalysts after various treatments.

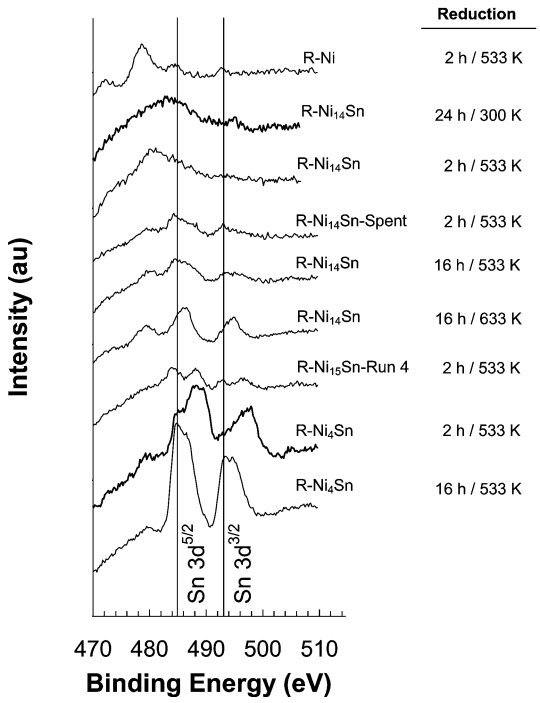

Fig. 3. Sn 3d region of X-ray photoelectron spectra of R-NiSn catalysts after various treatments.

near 854 eV [11,12] and previous studies of aqueous treatment of Ni catalysts have detected $Ni(OH)_2 \cdot xH_2O$ species near 856 eV [13]. Alternatively, this line at 856.4 eV may be a nickel acetate species, such as $Ni(OAc)_2 \cdot 4H_2O$, that has been observed between 856.3 and 856.7 eV. These Ni acetate species may be formed by reaction with the tributyltin acetate ligands during Sn promotion of the R-Ni catalyst. Nickel aluminate species have been observed with a Ni bind-

Table 1
Surface composition and binding energy of each species determined by X-ray photoelectron spectroscopy of R-Ni-based catalysts after various treatments

	Treatment	Ni	Ni^{x+}	Sn	Sn^{x+}	$–CH_2–$	$–CH_3$, C=O	O=C–O	Al^{x+}	O	Ni/Sn ratio	Ni/(Ni + Ni^x) (%)	Sn/(Sn + Sn^x) (%)
(a) Atomic composition (%)													
R-Ni	H_2/533 K/2 h	16.0		0.09			11.7	8.5	17.0	46.8	186	100	100
R-Ni_{14}Sn	air dried		10.1	0.07		12.7	4.4	2.2	12.8	57.8	138	0	100
R-Ni_{14}Sn	H_2/533 K/2 h	3.9	8.0	0.05		4.6	16.2	2.4	15.0	49.4	221	33	100
R-Ni_{14}Sn-Spent	H_2/533 K/2 h	4.9	4.1	0.36	0.21		5.7	11.9	7.0	66.0	15.9	55	64
R-Ni_{14}Sn	H_2/533 K/16 h	2.4	4.8	0.31	0.28		13.3	5.8	18.0	54.5	12.1	33	52
R-Ni_{14}Sn	H_2/633 K/16 h	4.5	3.4	0.41	0.68		20.9	2.4	16.1	51.7	7.2	57	37
R-Ni_{15}Sn-Run 4	H_2/533 K/2 h	4.2	7.2	0.45	0.45	1.4	12.0	6.8	9.0	58.0	12.8	37	50
R-Ni_4Sn	H_2/533 K/2 h	4.0	5.0	0.45	1.66		12.9	15.3	12.0	49.0	4.3	44	21
R-Ni_4Sn	H_2/533 K/16 h	8.9	3.3	2.53	2.06		22.7	5.6	13.0	41.9	2.7	73	55
(b) Binding energies (eV)													
R-Ni	H_2/533 K/2 h	852.5		484.3			285.5	288.2	77.0	533.3			
R-Ni_{14}Sn	air dried		856.2	484.7		282.1	285.8	290.0	75.0	531.8			
R-Ni_{14}Sn	H_2/533 K/2 h	852.7	856.2	484.7		282.5	286.7	290.0	76.2	532.3			
R-Ni_{14}Sn-Spent	H_2/533 K/2 h	852.8	856.0	484.5	487.0	282.5	285.8	288.0	74.7, 77.6	532.0, 534.8			
R-Ni_{14}Sn	H_2/533 K/16 h	853.0	857.0	484.5	486.9		285.8	288.7	74.8, 77.0	532.4			
R-Ni_{14}Sn	H_2/633 K/16 h	852.7	855.8	484.8	486.6		285.3	288.3	74.4	531.3			
R-Ni_{15}Sn-Run 4	H_2/533 K/2 h	852.8	856.0	484.1	488.0	283.0	285.4	288.6	74.8, 77.1	531.8, 535.1			
R-Ni_4Sn	H_2/533 K/2 h	853.0	857.4	485.0	488.5		286.0	288.3	77.1	531.3, 533.8			
R-Ni_4Sn	H_2/533 K/16 h	852.8	856.0	484.8	487.0		285.4	288.3	74.7	531.8			

ing energy of 856.0 eV [14], and some of this spinel may form during heat treatment.

Fig. 2 shows that the surface Ni in R-NiSn catalysts is more difficult to reduce than that in R-Ni catalysts. Treatment of R-Ni_{14}Sn at 533 K for 2 h in flowing H_2 gave an extent of reduction of only 33%, and this extent did not change when the treatment was maintained for 16 h (Table 1). Reduction at 633 K for 16 h led to a Ni reduction of 57%. Reduction of Ni is slightly easier in the higher-tin-content R-Ni_4Sn catalyst, with a value of 44% after a 2-h treatment in H_2 at 533 K. Continuing the treatment at 533 K for 16 h increased the extent of Ni reduction to 73%. The ongoing reduction of Ni in this R-Ni_4Sn catalyst may be concurrent with the formation of a NiSn surface alloy, as NiSn alloys are indistinguishable by XPS from reduced Ni surfaces [15–17]. Small amounts of NiAl alloy from the original synthesis of the R-Ni catalyst may also be present on the catalyst surface [18].

Fig. 3 shows the Sn 3d region of the R-NiSn catalysts. A Sn^0 peak at 484.7 eV is largest for the catalyst with the highest Sn content (R-Ni_4Sn) and grew with increasingly severe treatments in H_2. This reduced Sn species is likely a NiSn alloy, because pure Sn is known to reduce only above 800 K [17]. The higher binding energy Sn $3d^{5/2}$ peak is attributable to tin oxides (Sn^{2+} or Sn^{4+}), which are typically found near 486.5 eV [15,17,19], but which may shift to binding energies above 487 eV because of interaction with acetate or water-derived species. Mössbauer spectroscopy and SEM X-ray microanalyses have observed the migration of Sn to form Sn oxides associated with the surface alumina phase in R-Ni_{14}Sn catalysts [7–9]. Such behavior has been observed for Sn/Al_2O_3 catalysts that showed a Sn $3d^{5/2}$ peak at 487.3 eV due to the formation of tin aluminate after reduction at 673 K [20]. Some contribution to the high-binding-energy Sn peak may originate from alkyl tin compounds, since the Sn $3d^{5/2}$ band of Sn(n-C_4H_9)$_4$ has been observed at a binding energy of 486.2 eV [11]. Furthermore, decomposition of this tetrabutyltin compound on Rh/SiO_2 to form Rh(Sn(n-C_4H_9)$_x$)$_y$ surface complexes has been observed to raise this binding energy to 486.6 eV [21]. We note incidental peaks with binding energies near 480 eV due to a Ni LMM Auger transition.

The C 1s region of the XPS spectrum was also collected for the same R-NiSn catalysts. Each catalyst exhibited a peak at 285.8 eV, near the standard carbon $1s^{1/2}$ binding energy of 284.7 eV, which is likely due to surface contamination or contributions from methyl groups in the tributyltin acetate or butyl ligands [22]. A high binding-energy peak between 288 and 290 eV is present for Sn-promoted catalysts after drying or mild reduction at 523 K for 2 h, and it may be due to acetate groups associated with the organometallic tin precursor [23]. Similarly, a low binding-energy peak appears for these catalysts near 282.5 eV that likely corresponds to CH_2 groups from tributyltin acetate. The peak near 286 eV may also be due to adsorbed carbon monoxide, because thin films of tributyltin acetate are known to decompose between 373 and 463 K, whereas the acetate ligand fully decomposes to yield CO at 573 K [24]. Transition metals such as Ni promote the decomposition of organometallic Sn compounds or their ligands at lower temperatures [25,26].

Table 1 gives the surface composition of the catalysts after each treatment. In each case, the most abundant surface element is oxygen, which is likely associated with Al as alumina. The observed Al/O ratio near 1:3 agrees well with

previous SEM and XRD results showing that R-Ni catalysts contain large amounts of Bayerite and Gibbsite alumina ($Al(OH)_3$) that partially dehydrate after heat treatment in H_2 [7,8,27,28]. Furthermore, the observed Al 2p line at 74.7 eV agrees well with previous studies of hydrated alumina [29].

The surface concentration of Sn appears to be low on dried R-Ni_{14}Sn, perhaps because of poor dispersion of Sn species on the catalyst surface before heat treatment because reduction increases the surface Sn content significantly. Accordingly, the surface of the R-Ni catalyst contains 16% Ni, and this percentage decreases to about 10% after the addition of Sn species. Reduction of the R-Ni_{14}Sn catalyst at 533 K for 16 h gives a surface stoichiometry similar to that of the bulk material (Ni/Sn ratio = 12.1), whereas treatment at 633 K leads to surface enrichment (Ni/Sn ratio = 7.2). Similarly, reduction of R-Ni_4Sn at 533 K for 2 h leads to a Ni/Sn ratio of 4.3, whereas treatment at this temperature for 16 h gives a Ni/Sn ratio near 2.7. The apparent lack of Sn in the fresh catalyst may also be due to coverage of the Sn by its ligands.

3.3. Deactivation kinetics

Previous work [8] has shown that supported nickel catalysts exhibit severe deactivation during APR of ethylene glycol solutions at temperatures near 500 K. For example, catalysts composed of Ni supported on Al_2O_3, SiO_2, and ZrO_2 lost 90% of their initial activity over a period of 2 days at 498 K. Similarly, Ni_9Sn/Al_2O_3 loses nearly 90% of its catalytic activity after 48 h at 498 K. Skeletal Ni catalysts, such as Raney-Ni, show better stability, losing only about 50% of their activity over the same period. The addition of Sn also improves catalyst stability, such that R-Ni_{14}Sn catalysts lose only 30% of their activity over 48 h at 498 K during APR of 10 wt% ethylene glycol solutions, implying a first-order deactivation constant (k_d) of 0.0026 h^{-1}. Subsequent calcination at 573 K in flowing O_2 followed by reduction at 523 K in H_2 did not restore catalytic activity.

Fig. 4 shows the performance of a R-Ni_{15}Sn catalyst versus time on stream for aqueous-phase reforming of various ethylene glycol (EG) solutions at 483 K. A standard case for reforming of 5 wt% EG after reduction of the catalyst at 523 K is labeled as Run 1 (see Table 2). During this run, deactivation occurs rapidly over the first 24 h, followed by periods of slower deactivation for times between 24–140 h ($k_d = 0.0026\ h^{-1}$) and 140–240 h ($k_d = 0.0020\ h^{-1}$). Run 2 shows that the catalyst is more stable after more extensive catalyst pretreatment in H_2 (16 h at 623 K), with deactivation constants of 0.0016 and 0.0014 h^{-1} for the above two time periods, respectively. Run 3 was conducted with a stoichiometric feed containing 63 wt% ethylene glycol after reduction of the catalyst at 523 K. Under these conditions, the catalyst exhibits slow deactivation between 24 and 140 h ($k_d = 0.0008\ h^{-1}$) and nearly constant catalytic activity through at least 280 h ($k_d = 0.0001\ h^{-1}$). Run 4 combines reduction at 623 K (Run 2) with stoichiometric feed (Run 3) for long-term stability ($k_d = -0.0005\ h^{-1}$ between 140 and 240 h). Thus, it appears that the presence of excess water in the feed is responsible for some of the deactivation observed in Runs 1 and 2.

The APR of concentrated ethylene glycol feeds leads to lower catalytic activity and selectivity for H_2 production. Table 2 shows that the initial rate of H_2 production decreases from 94.1 to 19.4 $\mu mol\ g_{cat}^{-1}\ min^{-1}$ during Runs 1 and 3, respectively. The hydrogen selectivity decreases from 74.0 to 60.9%. Reduction at 623 K increases the activity of the catalyst for APR of the stoichiometric feed, increasing the rate of H_2 production to 28.2 and 21.6 $\mu mol\ g_{cat}^{-1}\ min^{-1}$ initially and after 240 h, respectively. Thus, a reduction in catalyst

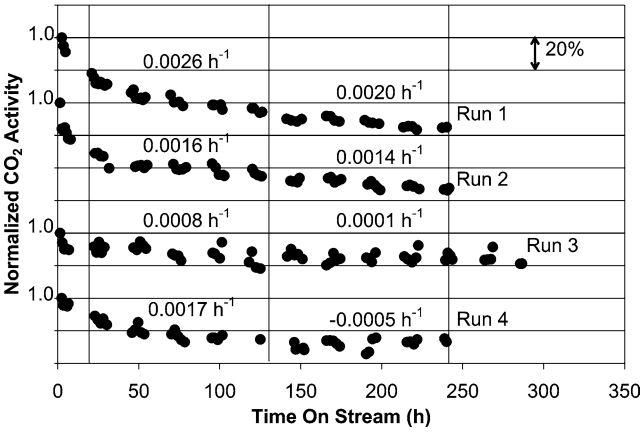

Fig. 4. Deactivation profiles for aqueous phase reforming of various ethylene glycol solutions over R-Ni_{15}Sn at 483 K (see Table 2 for details).

Table 2
Kinetics results for reforming of ethylene glycol solutions at 483 K over R-Ni_{15}Sn catalysts. Values are recorded after 6 h time on stream (left) and after 240 h time on stream (right)

Run	H_2 reduction		Feed (wt%)	Press (bar)	LHSV[a] (h^{-1})	Conversion %C to gas	Production rate ($\mu mol\ min^{-1}\ g_{cat}^{-1}$)						CO/CO_2 ratio	Selectivity	
	Time (h)	Temp. (K)					CO	CO_2	CH_4	C_2H_6	H_2	Total H_2[b]		Alkane (%)	H_2 (%)
1	2	523	5	19.6	8.33	34.1/13.8	0.2/0.1	43.9/19.7	5.9/0.8	0.3/0.0	94.1/48.7	120.5/52.0	0.004/0.004	13.2/4.0	74.0/94.5
2	16	623	5	19.6	7.19	26.9/11.5	0.2/0.1	31.2/14.4	2.9/0.3	0.2/0.0	61.6/37.8	74.6/38.8	0.005/0.005	9.5/1.7	71.2/102.6
3	2	523	63	14	0.93	6.1/4.5	1.2/1.2	8.3/7.2	2.3/0.9	0.2/0.1	19.4/15.1	31.8/19.6	0.139/0.165	25.4/12.0	60.9/63.5
4	16	623	63	14	7.20	0.9/0.6	1.0/1.1	10.6/8.1	2.2/0.6	0.2/0.0	28.2/21.6	38.6/24.1	0.094/0.138	18.7/6.5	79.2/87.2

[a] Liquid hourly space velocity (LHSV, h^{-1}) defined as (volumetric flow rate of feed solution ($cm^3\ h^{-1}$))/(catalyst bed volume (cm^3)).
[b] Amount of H_2 that would be generated if all gaseous carbon products had been CO_2.

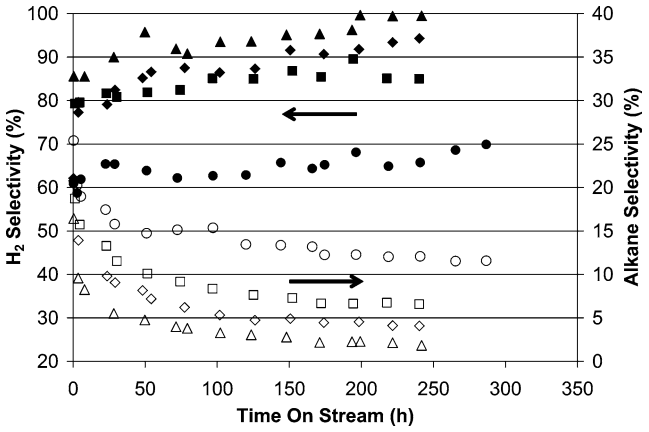

Fig. 5. Variation of the H_2 (solid symbols) and alkane selectivities (open symbols) with time-on-stream for reforming of ethylene glycol solutions during Run 1 (♦), Run 2 (▲), Run 3 (●), and Run 4 (■) over R-Ni_{15}Sn at 483 K (see Table 2 for details).

activity during Runs 3 and 4 is offset by an improvement in catalytic stability.

During APR of concentrated feed stocks there is insufficient water to achieve equilibrium for the water gas shift reaction ($CO + H_2O \leftrightarrow H_2 + CO_2$). For example, the measured CO/CO_2 product ratio is 0.17 for Run 3 compared with 0.004 for Run 1, and we estimate that the equilibrium CO/CO_2 ratios are equal to 0.0003 and 0.0002 for these two runs, respectively (Table 2) [5]. We suggest that the larger amount of CO generated in Run 3 produces CH_4 upon hydrogenation, leading to lower H_2 selectivities. We have previously shown that methane production can be controlled by a change in the tin loading of the catalyst, a decrease in the residence time in the reactor, and/or a decrease in the CO and H_2 partial pressures in the reactor [8].

Fig. 5 shows that the H_2 selectivity of each catalyst increases over the first 50 h on stream, and the alkane selectivity decreases correspondingly. Accordingly, the more severe treatment in H_2 of R-Ni_{15}Sn in Run 2 leads to higher H_2 selectivity and lower alkane selectivity compared with Run 1, that is, initial H_2 and alkane selectivities of 86 and 16% for Run 2 compared with 62 and 21% for Run 1, respectively. Exposure to reaction conditions causes a further improvement in hydrogen selectivity after 240 h on stream, perhaps because of more extensive formation of NiSn alloys. Similarly, catalyst pretreatment at 623 K and lower reactor residence time improve the APR of the stoichiometric feed. A combination of concentrated feed and high-temperature pretreatment leads to an improved initial hydrogen selectivity of 79.2% during Run 4. Catalyst aging further improves the selectivity to 87.2% after 240 h on stream (Table 2).

Fig. 6A shows that Ni is leached from the catalyst at a significant rate during Runs 1 and 2, rising to near 50 wppm after 240 h on stream. The effluent Ni concentration can be decreased to 10 wppm or less through a limit on the water content of the feed (Runs 3 and 4). Conversely, Fig. 6B shows that elution of Sn is slow for Runs 1 and 2 (less than 8 wppm) and faster for Runs 3 and 4 (40–60 wppm). Our

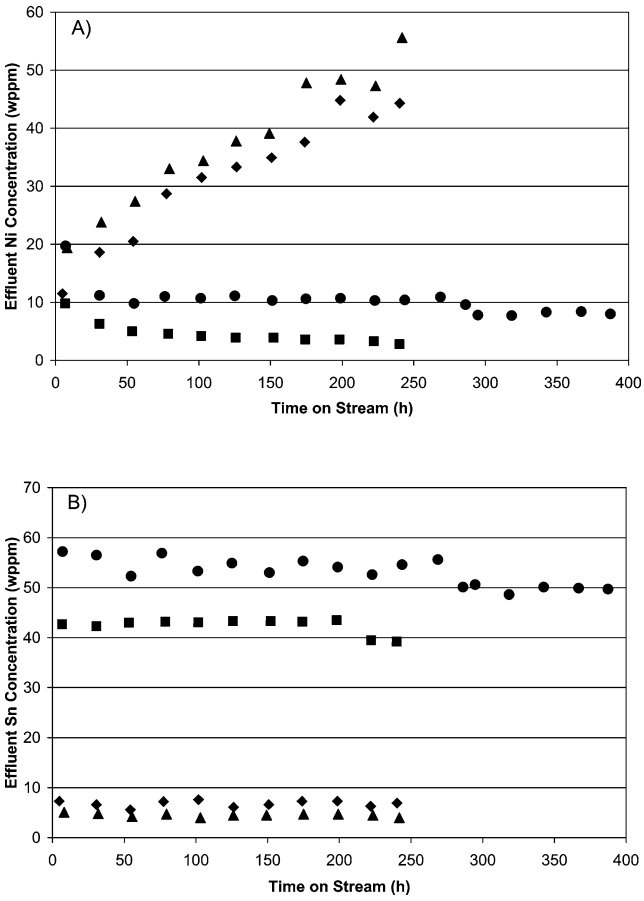

Fig. 6. Variation of effluent (A) Ni and (B) Sn concentrations with time-on-stream for reforming of ethylene glycol solutions during Run 1 (♦), Run 2 (▲), Run 3 (●), and Run 4 (■) over R-Ni_{15}Sn at 483 K.

XPS studies indicate that residual AlO_x species from the production of R-Ni catalysts by caustic leaching of NiAl alloys are present on the catalyst surface, and SEM studies have shown the crystallization of Al-rich phases on the surface after hydrothermal treatments [8,28]. These alumina species elute more slowly than Ni or Sn (Al effluent concentrations of 1–3 wppm).

3.4. Characterization of catalysts after reaction kinetics measurements

Results of R-Ni_{15}Sn characterization before and after Runs 1–4 are listed in Table 3. The CO adsorption uptake and BET surface area decrease with high-temperature reduction at 623 K, accompanied by a slight increase in Ni particle size indicated by XRD. The CO uptake and surface area decrease further upon exposure to reaction conditions at 483 K, and nickel particle sizes remain in the range of 40–50 nm. The loss in CO adsorption capacity and surface area is most severe for APR of dilute ethylene glycol solutions after mild reduction at 523 K, falling from 223 μmol g_{cat}^{-1} and 74.3 $m^2\ g_{cat}^{-1}$ to 134 μmol g_{cat}^{-1} and 40.9 $m^2\ g_{cat}^{-1}$, respectively, during Run 1. In comparison, the CO uptake and surface

Table 3
Characterization of freshly reduced (left) and spent (right) R-$Ni_{15}Sn$ catalysts before and after Runs 1–4

Run	Reduction		Reaction conditions				Characterization		
	Temp. (K)	Time (h)	Feed (wt%)	Press. (bar)	LHSV (h^{-1})	TOS (h)	CO uptake ($\mu mol\ g_{cat}^{-1}$)	BET area ($m^2\ g^{-1}$)	Ni part. size[a] (nm)
1	523	2	5	19.6	8.33	240	223/134	74.3/40.9	47/49
2	623	16	5	19.6	7.19	242	166/154	61.0/48.2	52/46
3	523	2	63	14	0.93	387	223/165	74.3/56.9	47/40
4	623	16	63	14	7.2	240	166/167	61.0/65.6	52/49

[a] Determined by XRD.

area remain nearly constant at 166–167 μmol g_{cat}^{-1} and 61.0–65.6 $m^2\ g_{cat}^{-1}$, respectively, during Run 4.

In situ X-ray photoelectron spectroscopy was used to investigate the surface state of R-NiSn catalysts after reaction and re-reduction at 523 K for 2 h. The core-level Ni spectra of spent R-$Ni_{14}Sn$ (10 wt% ethylene glycol solution at 498 K for 48 h) and R-$Ni_{15}Sn$ (Run 4) are compared with those of similar fresh R-NiSn catalysts in Fig. 2 (Table 1). The spent R-$Ni_{14}Sn$ catalyst contains a combination of 55% reduced Ni, presumably as NiSn alloy (852.8 eV), and 45% $Ni(OH)_2$ (856.0 eV). Spent R-$Ni_{15}Sn$ from Run 4 contains 37% reduced Ni and 63% $Ni(OH)_2$, similar to the extent of reduction of fresh R-$Ni_{14}Sn$ catalysts after reduction between 523 and 623 K. Thus, R-NiSn catalysts appear to be partially oxidized during APR reaction conditions near 500 K.

X-ray photoelectron spectra for the Sn 3d region of the spent R-NiSn catalysts are shown in Fig. 3. The spent R-$Ni_{14}Sn$ catalyst contains a mixture of 64% reduced Sn (Sn $3d^{5/2}$ at 484.5 eV) as a NiSn alloy and 36% SnO_x (487.0 eV). The tin in this catalyst has undergone a degree of reduction similar to that of fresh reduced R-$Ni_{14}Sn$ (52%). The tin in the spent R-$Ni_{15}Sn$ is less reduced (50%), which is similar to the state of tin in R-$Ni_{14}Sn$ reduced at 633 K. However, the oxidized Sn species in spent R-$Ni_{15}Sn$ is at a very high binding energy of 488.0 eV, suggesting the formation of tin organometallic compounds such as tin acetate.

Table 1 shows that the surfaces of the two spent catalysts are composed of about 10% Ni, similar to fresh reduced catalysts. However, the Ni/Sn ratio of the spent $Ni_{14}Sn$ catalyst falls to 15.9, so tin enrichment of the surface occurs during reaction conditions for 48 h at 498 K. Furthermore, the surface aluminum content of the spent catalysts is significantly lower than that of fresh materials, consistent with observation of poorly dispersed alumina crystallites on the spent R-$Ni_{14}Sn$ catalyst by SEM [7]. We note that the Ni–C surface ratio of the spent catalysts is similar to that of fresh reduced R-$Ni_{14}Sn$ catalysts, indicating that coking of the catalysts does not occur during reaction. The carbon species appear to be hydrocarbons or carbon monoxide at 285.4 eV and acetate species between 288 and 289 eV.

3.5. Thermogravimetric analysis

Thermogravimetric analysis of R-Ni-based catalysts under flowing N_2 was done to dry the samples and allow for thermal decomposition/desorption of adsorbed species. Subsequent thermogravimetric analysis of the catalysts under flowing air gave several positive peaks corresponding to the oxidation of various components. Passivated R-Ni undergoes bulk oxidation at 560 K, and this peak shifts to higher temperatures for reduced and spent R-$Ni_{15}Sn$ catalysts, perhaps because of NiSn alloys that are known to be more resistant to oxidation than pure Ni [30]. Small peaks near 340 K may be due to oxidation of Sn or SnO on the surface of spent catalysts. We note that no negative peaks are observed during the temperature ramp under flowing air that would denote a loss of mass associated with oxidation of coke on the catalyst surface.

4. Discussion

4.1. NiSn particle model

Characterization of the R-Ni catalysts by SEM [7,8] shows that R-Ni contains a porous Ni surface covered by alumina crystallites. X-ray photoelectron spectroscopy indicates that addition of Sn to this surface by controlled surface reaction of tributyltin acetate leads to a diffuse covering of carbon-rich surface species. After heat treatment for at least 16 h at 533 K, the organometallic compound decomposes and tin migrates into Ni particles to form a Ni_3Sn phase identified by Mössbauer spectroscopy [7,8] around a core of Ni observed by XRD. Residual Sn associates with surface alumina to form mixed Al–Sn oxides.

Addition of Sn to Ni catalysts significantly decreases the reactivity of the surface, as indicated by the reduced adsorption heat and uptake of CO and H_2. This weakened adsorption behavior may be due to the presence of Ni_3Sn or selective poisoning by Sn of Ni defect or edge sites. Tin enrichment of the surface region observed in spent catalysts by XPS agrees well with surface science studies of stable, Sn-rich NiSn surface alloys, such as buckled $p(\sqrt{3}\times\sqrt{3})R30^\circ$ Sn/Ni(111) [31] (Ni_2Sn stoichiometry) or $c(2\times 2)$ Sn/Ni(001) [32]. Adsorption of CO on Ni(111) is favored at threefold-hollow sites [33] and is strongly suppressed on $p(\sqrt{3}\times\sqrt{3})R30^\circ$ Sn/Ni(111) surfaces that have no suitable Ni ensembles [34]. Similarly, NiSn alloys adsorb H_2 much more weakly than does Ni [35,36], and the effect of Sn addition to Ni is even larger for adsorption of H_2 than CO.

We also note that the differential heat plots given in Fig. 1 are smooth and continuous, indicating a homogeneous surface, and we conclude that the active phase of R-NiSn catalysts is a surface NiSn alloy. This Sn-rich layer covers a Ni core that forms the bulk of the material.

4.2. Catalyst deactivation by sintering

Deactivation of R-NiSn catalysts appears to be dominated by interactions with water during APR of oxygenated hydrocarbon solution at 483 K. Over a period of about 48 h, the catalysts suffer from sintering of the most highly dispersed metal particles on R-Ni, concurrent with a decrease in the surface area and CO uptake of the catalyst. X-ray diffraction patterns indicate that fresh R-NiSn catalysts are composed of Ni particles with sizes near 38 nm [8]. After APR of 10 wt% ethylene glycol solutions at 498 K, the particles of R-$Ni_{14}Sn$ appear to grow slightly to about 40 nm. In contrast, Ni/Al_2O_3 catalysts show significant narrowing of the diffraction peaks, indicating an increase in the Ni particle size from 7 to 125 nm according to the Scherrer equation after similar exposure to reaction conditions. Addition of Sn slows the growth of alumina-supported Ni crystallites, as spent Ni_9Sn/Al_2O_3 is composed of 38-nm particles.

The X-ray diffraction patterns of R-$Ni_{15}Sn$ catalysts are similar before and after exposure to various APR reaction conditions, as indicated in Table 3. Reduction of the fresh catalyst at 523 K leads to a Ni particle size of 47 nm compared with 38 nm for R-Ni after the same treatment. The Ni particles in R-$Ni_{15}Sn$ grow to 52 nm after reduction at 623 K but remain near 40–50 nm after reaction for over 240 h at 483 K. A shoulder on the Ni peak near $2\theta = 44°$ indicates the formation of NiSn alloys, as observed by Mössbauer spectroscopy of spent R-$Ni_{14}Sn$ catalysts [7,8].

Consistent with our current results, prior studies [7,8] have shown that fresh R-Ni is a high-surface-area material consisting of reduced Ni particles. After drying and passivation in 2% O_2/He at 300 K, R-Ni has a BET surface area of 105 $m^2\,g^{-1}$. Treatment in H_2 at 523 for 2 h decreases the surface area to 46 $m^2\,g^{-1}$, with an irreversible CO chemisorption uptake of 222 $\mu mol\,g^{-1}$. Addition of Sn to R-Ni decreases the surface area of the catalyst slightly, with some evidence of pore blocking in R-Ni_4Sn (31.9 $m^2\,g^{-1}$). The CO and H_2 uptake decrease to a greater extent than the surface area as Sn is added to R-Ni, with uptakes of 57.1 and 10.2 $\mu mol\,g^{-1}$, respectively, for R-Ni_4Sn.

Exposure to APR reaction conditions at 483 K causes a decrease in the extent of CO adsorption on R-$Ni_{15}Sn$. Some of the loss of CO adsorption capacity during Run 1 is due to the effect of water on the catalyst, because a CO uptake of 165 $\mu mol\,g^{-1}$ is observed after reforming of 63% ethylene glycol solutions during Run 3. Although catalyst reduction at 623 K for 16 h leads to a lower initial uptake of 166 $\mu mol\,g^{-1}$, these catalysts are more stable with respect to time on stream during APR of both dilute (Run 2, 154 $\mu mol\,g^{-1}$) and concentrated (Run 4, 167 $\mu mol\,g^{-1}$) feeds, indicating that a portion of the degradation of the catalyst during Run 1 is due to exposure to the reaction temperature for long periods of time. We note that the BET surface area follows trends similar to that of CO adsorption with reduction temperature. The BET surface area decreases from 74.3 to 56.9 $m^2\,g^{-1}$ during Run 3 and increases slightly from 61.0 to 65.6 $m^2\,g^{-1}$ during Run 4. The increase in adsorption capacity during Run 4 may be due to removal of Sn from the pores of R-$N_{15}Sn$, as discussed below.

4.3. Leaching of metals

Reduced Ni particles lose catalytic activity and gain mobility under hydrothermal conditions by oxidation and hydration to form $Ni(OH)_2$, as observed by XPS [13,37]. $Ni(OH)_2$ forms a nearly passive layer in water ($K_{sp} = 2.0 \times 10^{-15}$ at 298 K) that may only be dissolved by strongly acidic or basic solutions [38,39]. Nickel may also leach into the reactor effluent by action of acids that may be present as by-products of the reforming process, such as dilute carbonic (e.g., dissolved CO_2) and acetic acids [40]. We note that fresh R-Ni catalysts can be stored in a reduced state under dilute caustic solutions for months [41],

$$\mathrm{Ni_{(s)} \xrightarrow{O_2/H_2O} NiO_{(s)} \xrightarrow{H_2O} Ni(OH)_{2(s)} \xrightarrow{H^+/OH^-} Ni^{2+}_{(aq)} + 2OH^-_{(aq)}}. \qquad (4)$$

$$\mathrm{H^+}$$

Tin can be oxidized and/or hydrated by water [42] to form highly passive $Sn(OH)_2$ ($K_{sp} = 1.4 \times 10^{-28}$ at 298 K) or SnO_2. Consquently, we suggest that the tin elution is caused primarily by dissolution of organometallic tin compounds that are more soluble in ethylene glycol than water. These organometallic compounds may be formed by reactions of tin with ethylene glycol or reaction intermediates that form in the reforming process [43]. Reforming of feed solutions with intermediate oxygenate concentrations (e.g., 20–30 wt%) may minimize the leaching of Ni and Sn species.

After several days on stream, catalyst deactivation continues at a slower rate because of interaction between water and the NiSn surface. Slow oxidation/hydration and sintering by water between 140 and 240 h on stream can be mitigated by the use of stoichiometric feeds, leading to nearly stable operation over long periods of time ($k_d = 0.0001$ vs 0.0020 h^{-1} for reforming of 63 and 5% ethylene glycol solutions, respectively). The use of stoichiometric feeds is also beneficial to the overall energy efficiency of the system because no excess water must be processed in the APR reactor. Thorough alloy formation by treatment further improves the long-term stability of the catalyst for reforming of dilute (Run 2: $k_d = 0.0014\ h^{-1}$) and stoichiometric (Run 4: $k_d = -0.0005\ h^{-1}$) feed stocks, perhaps by maintaining high surface areas and surface site densities.

Tin may suppress sintering and dissolution of Ni by improving the oxidation resistance of Ni surfaces. Using temperature-programmed reduction (TPR), Nichio et al. [30] have shown that adding as little as 0.04% Sn to 2 wt% Ni/

α-Al_2O_3 lowers the reduction temperature from about 873 K for the Ni catalyst to near 723 K for the intermetallic compound. Padeste et al. [15] used XPS to verify that SnO_2 reduces more easily when it is added to NiO/α-Al_2O_3 than when it is added to α-Al_2O_3. Thus, a synergistic effect is seen in Ni–Sn alloys, as the intermetallic compound reduces more easily than Ni or Sn alone on alumina supports. In fact, Ni–Sn surfaces are known to be highly corrosion resistant [44]. Commercial Ni–Sn cathodes for the hydrogen evolution side of the chlor-alkali process are stable in 32 wt% NaOH solution at 358 K [45,46].

4.4. Coking and carbonyl formation

Nickel catalysts are vulnerable to strong interactions with the APR feed stock and products, notably carbon monoxide. Hydrogenation of CO proceeds on Ni surfaces by dissociation of the C–O bond followed by hydrogenation of the carbon fragment [47], but carbon deposits can cover the Ni surface as single atoms (C_α), surface films (C_β), carbonaceous polymers, filamentary strands, or graphitic species (C_γ) [48]. Coking tends to occur at high temperature (> 600 K) and low H_2O/C ratios in steam reforming of alkanes [49]. Importantly, we note that thermogravimetric analysis and XPS surface carbon measurements revealed that significant amounts of coke were not present on the spent R-$Ni_{15}Sn$ catalysts.

The beneficial effect of Sn on the APR selectivity of Ni catalysts for hydrogen rather than alkanes may coincide with improved coking resistance. In this respect, dissociation of CO leading to formation of methane over Ni may take place preferentially on Ni-defect sites [50], so the decoration of defect sites by Sn may suppress methanation reactions. It is also possible that methanation reactions are suppressed by geometric effects caused by the presence of Sn on Ni–Sn alloy surfaces, that is, by decreasing the number of surface ensembles composed of multiple nickel atoms that are necessary for CO or H_2 dissociation [34].

The production of gaseous or adsorbed CO by the APR process may lead to formation of volatile Ni carbonyl species by the following reaction:

$$\mathrm{Ni} + 4\mathrm{CO}_{(g)} \rightleftarrows \mathrm{Ni(CO)}_{4(g)}. \quad (5)$$

These $Ni(CO)_4$ species are most stable at low temperatures, with an equilibrium constant near 10^{-6} at 483 K. Using this value, we calculate [2,5] a $Ni(CO)_4$ partial pressure of 2×10^{-13} Pa during the run at a system pressure 1 bar above the bubble-point of the 5 wt% ethylene glycol feed. This value is well below the maximum of 10^{-6} Pa quoted by Shen et al. [51] for stable operation of Ni/Al_2O_3 catalysts under methanation reaction conditions. However, the calculated nickel carbonyl partial pressure increases to about 10^{-6} Pa for the 63 wt% ethylene glycol feed, suggesting that particle growth by carbonyl transport may be active for concentrated feeds and at high system pressures, especially because particle growth by carbonyl transport may occur with sub-carbonyl species with fewer CO ligands [52]. This possible sintering mechanism may be suppressed by Sn, since we have observed that addition of Sn to R-Ni causes a decrease in the heat of CO adsorption.

5. Conclusions

Results from X-ray photoelectron spectroscopy indicate that addition of Sn to R-Ni catalysts by controlled surface reaction of tributyltin acetate leads to a partially reduced NiSn surface after treatments in H_2 of up to 16 h at 633 K. The organometallic compound decomposes at temperatures above 533 K and leads to a tin-rich surface after further heat treatment. The Sn-rich surface surrounds a core of Ni observed by XRD. Microcalorimetry of CO and H_2 adsorption show that the Sn-covered surface adsorbs these molecules more weakly than Ni alone, in good agreement with surface science studies of NiSn alloys, such as buckled $p(\sqrt{3} \times \sqrt{3})R30°$ Sn/Ni(111) (Ni_2Sn stoichiometry). Our XPS results suggest that residual Sn associates with surface alumina to form mixed Al–Sn oxides, but BET and XRD results confirm that residual Sn species do not reduce the surface area by pore blocking or particle growth.

Deactivation of R-NiSn catalysts is dominated by interactions with water during the APR reaction, as thermogravimetric analysis and XPS showed that detectable amounts of coke were not present on spent R-$Ni_{15}Sn$ catalysts. Over a period of about 48 h, the catalysts suffer from sintering of the most highly dispersed metal particles on R-Ni, concurrent with a decrease in the surface area and CO uptake of the catalyst. After several days on stream, catalyst deactivation continues at a slower rate because of interaction between water and the oxidation-resistant NiSn surface. Slow oxidation/hydration and sintering by water between 140 and 240 h on stream can be mitigated by the use of stoichiometric feeds, leading to nearly stable operation over long periods of time ($k_d = 0.0001$ vs 0.0020 h^{-1} for reforming of 63 and 5% ethylene glycol solutions, respectively). Thorough alloy formation by treatment in H_2 further improves the long-term stability of the catalyst for reforming of dilute ($k_d = 0.0014$ h^{-1}) and stoichiometric ($k_d = -0.0005$ h^{-1}) feed stocks by maintaining high surface areas and surface site densities.

Leaching of Ni and Sn metals into the reactor effluent occurs during aqueous phase reforming at 483 K. For reforming of dilute feed stocks, the Ni concentration in the effluent increases from 10–50 wppm over 240 h on stream, whereas the Sn concentration remains constant below 10 wppm. This behavior may be due to hydration and dissolution of NiO through a $Ni(OH)_2$ species on the catalyst surface identified by XPS. For reforming of concentrated solutions, the Sn concentration is 30–50 ppm, perhaps because of formation of organometallic compounds with ethylene glycol, whereas the Ni concentration is below 10 ppm. A feed consisting

of 20–30 wt% ethylene glycol may therefore minimize the combined Ni and Sn elution.

The results of this study demonstrate that R-NiSn catalysts can be used for stable, long-term generation of H_2 by aqueous-phase reforming processes. To achieve the best stability versus time on stream, it is necessary to reduce the impact of water on the physical stability of the catalyst, with the use of rigorous heat treatments in H_2 to form resilient NiSn alloys before reaction and/or with the use of concentrated feeds. Thorough alloy formation leads to hydrogen selectivities near 90% over R-$Ni_{15}Sn$, whereas the use of stoichiometric feeds represents a major improvement in the overall energy efficiency of the APR process compared with the generation of hydrogen from dilute feed solutions.

Acknowledgments

This work was supported by the US Department of Energy (DOE), Office of Basic Energy Sciences, Chemical Sciences Division. We also acknowledge funding from the Energy Center of Wisconsin and the University of Wisconsin Office of University-Industrial Relations. We thank George Huber for helpful discussions.

References

[1] R.D. Cortright, R.R. Davda, J.A. Dumesic, Nature 418 (2002) 64.
[2] R.R. Davda, J.A. Dumesic, Ang. Chem., Int. Ed. 42 (2003) 4068.
[3] R.R. Davda, J.A. Dumesic, Chem. Commun. 1 (2004) 36.
[4] R.R. Davda, J.W. Shabaker, G.W. Huber, R.D. Cortright, J.A. Dumesic, Appl. Catal. B 43 (2002) 13.
[5] J.W. Shabaker, G.W. Huber, R.R. Davda, R.D. Cortright, J.A. Dumesic, J. Catal. 215 (2003) 344.
[6] J.W. Shabaker, G.W. Huber, R.R. Davda, R.D. Cortright, J.A. Dumesic, Catal. Lett. 88 (2003) 1.
[7] G.W. Huber, J.W. Shabaker, J.A. Dumesic, Science 300 (2003) 2075 I.
[8] J.W. Shabaker, G.W. Huber, J.A. Dumesic, J. Catal. 222 (2004) 180.
[9] J.W. Shabaker, J.A. Dumesic, Ind. Eng. Chem. Res. 43 (2004) 3105.
[10] J. Shen, J.M. Hill, R.M. Watwe, B.E. Spiewak, J.A. Dumesic, J. Phys. Chem. 103 (1999) 3923.
[11] G.E. Moulder, W.F. Stickle, P.E. Sobol, K.D. Bomben, Handbook of X-Ray Photoelectron Spectroscopy, Perkin–Elmer, Physical Electronics Division, Wellesley, MA, 1992.
[12] C.D. Wagner, L.H. Gale, R.H. Raymond, Anal. Chem. 51 (1979) 466.
[13] Z.-L. Ma, R.-L. Jia, C.-J. Liu, J. Mol. Catal. A 210 (2004) 157.
[14] C.P. Li, A. Proctor, D.M. Hercules, Appl. Spectrosc. 38 (1984) 880.
[15] C. Padeste, D.L. Trimm, R.N. Lamb, Catal. Lett. 17 (1993) 333.
[16] A. Onda, T. Komatsu, T. Yashima, Chem. Commun. 15 (1998) 1507.
[17] A. Onda, T. Komatsu, T. Yashima, J. Catal. 201 (2001) 13.
[18] N.R. Gleason, S. Chaturvedi, D.R. Strongin, Surf. Sci. 326 (1995) 27.
[19] J. Arana, P.R.D.L. Piscina, J. Llorca, J. Sales, N. Homs, J.L.G. Fierro, Chem. Mater. 10 (1998) 1333.
[20] K. Balakrishnan, J. Schwank, J. Catal. 127 (1991) 287.
[21] B. Didillon, C. Houtman, T. Shay, J.P. Candy, J.M. Basset, J. Am. Chem. Soc. 115 (1993) 9380.
[22] M.A. Helfand, J.B. Mazzanti, M. Fone, R.H. Reamey, Langmuir 12 (1996) 1296.
[23] D. Briggs, M.P. Seah, Practical Surface Analysis, Wiley, Chichester, 1983.
[24] P.S. Patil, R.K. Kawar, S.B. Sadale, P.S. Chigare, Thin Solid Films 437 (2003) 34.
[25] O.A. Ferretti, L.C.B.D. Pauli, J.P. Candy, G. Mabillon, J.P. Bournonville, Stud. Surf. Sci. Catal. 31 (1987) 713.
[26] M. Agnelli, P. Louessard, A.E. Mansour, J.P. Candy, J.P. Bournonville, J.M. Basset, Catal. Today 6 (1989) 63.
[27] S. Gobolos, E. Talas, M. Hegedus, J.L. Margitfalvi, J. Ryczkowski, in: M. Guisnet, J. Barrault, C. Bouchoule, D. Duprez, G. Perot, R. Maurel, C. Montassier (Eds.), Heterogeneous Catalysis and Fine Chemicals Ii, vol. 335, Elsevier, Amsterdam, 1991.
[28] S.D. Robertson, J. Freel, R.B. Anderson, J. Catal. 24 (1972) 130.
[29] C.D. Wagner, H.A. Six, W.T. Jansen, J.A. Taylor, Appl. Surf. Sci. 9 (1981) 203.
[30] N.N. Nichio, M.L. Casella, G.F. Santori, E.N. Ponzi, O.A. Ferretti, Catal. Today 62 (2000) 231.
[31] S.H. Overbury, Y. Ku, Phys. Rev. B 46 (1992) 7868.
[32] L.-J. Chen, R. Wu, Surf. Sci. 345 (1996) L34.
[33] L. Becker, S. Aminpirooz, B. Hillert, M. Pedio, J. Haase, D.L. Adams, Phys. Rev. B 47 (1993) 9710.
[34] C. Xu, B.E. Koel, Surf. Sci. 327 (1995) 38.
[35] M. Finetti, E.E. Ottavianelli, R. Pis Diez, A.H. Jubert, Comp. Mat. Sci. 20 (2001) 57.
[36] M. Agnelli, J.P. Candy, J.M. Basset, J.P. Bournonville, O.A. Ferretti, J. Catal. 121 (1990) 236.
[37] C. Ludwig, W.H. Casey, J. Colloid Interface Sci. 178 (1996) 176.
[38] T.W. Swaddle, T.C.T. Wong, Can. J. Chem. 56 (1978) 363.
[39] R.C. Weast (Ed.), Handbook of Chemistry and Physics, CRC Press, Cleveland, OH, 1975.
[40] R.H. Perry, D.W. Green, Perry's Chemical Engineers' Handbook, McGraw–Hill, New York, 1984.
[41] P.J. Cerino, G. Fleche, P. Gallezot, J.P. Salome, in: M. Guisnet (Ed.), Heterogeneous Catalysis and Fine Chemicals Ii, vol. 231, Elsevier, Amsterdam, 1991.
[42] S.A. Awad, A. Kassab, J. Electroanal. Chem. 26 (1970) 127.
[43] K.G. Kochetikhina, G.A. Domrachev, G.A. Razuvaev, Zhurnal Obshchei Khimii 39 (1969) 1108.
[44] S.C. Britton, R.M. Angles, J. Electrodepositors' Tech. Soc. 27 (1951) 293.
[45] H. Yamashita, K. Yoshimoto, T. Yamamura, M. Fukuya, Electrochem. Soc. Proc. 93-14 (1993) 170.
[46] M. Fukuoka, H. Yamashita, K. Yoshimoto, Electrochem. Soc. Proc. 98-10 (1998) 304.
[47] A.D. Logan, M.T. Paffett, in: L. Guczi, et al. (Eds.), Catalysis at Experimentally Designed Surfaces: N-Butane Hydrogenolysis at Sn/Group Viii Surface Alloys, 10th International Congress on Catalysis, Budapest, Hungary, Elsevier, Amsterdam, 1993.
[48] C.H. Bartholomew, M.V. Strasburg, H.-Y. Hsieh, Appl. Catal. 36 (1988) 147.
[49] J.R. Rostrup-Nielsen, Steam Reforming Catalysts, Danish Technical Press, Inc., Copenhagen, Denmark, 1975.
[50] H.P. Steinruck, M.P. D'evelyn, R.J. Madix, Surf. Sci. 172 (1986) L561.
[51] W.M. Shen, J.A. Dumesic, C.G. Hill Jr., J. Catal. 68 (1981) 152.
[52] M. Agnelli, M. Kolb, C. Miradatos, J. Catal. 148 (1994) 9.